SANDIA REPORT

SAND2009-0536
Unlimited Release
Printed January 2009

Novel Ultrafine Grain Size Processing of Soft Magnetic Materials

Charles V. Robino and Joseph R. Michael

Prepared by
Sandia National Laboratories
Albuquerque, New Mexico 87185 and Livermore, California 94550

Sandia is a multiprogram laboratory operated by Sandia Corporation,
a Lockheed Martin Company, for the United States Department of Energy'
National Nuclear Security Administration under Contract DE-AC04-94AL85000.

Approved for public release; further dissemination unlimited.

Issued by Sandia National Laboratories, operated for the United States Department of Energy by Sandia Corporation.

NOTICE: This report was prepared as an account of work sponsored by an agency of the United States Government. Neither the United States Government, nor any agency thereof, nor any of their employees, nor any of their contractors, subcontractors, or their employees, make any warranty, express or implied, or assume any legal liability or responsibility for the accuracy, completeness, or usefulness of any information, apparatus, product, or process disclosed, or represent that its use would not infringe privately owned rights. Reference herein to any specific commercial product, process, or service by trade name, trademark, manufacturer, or otherwise, does not necessarily constitute or imply its endorsement, recommendation, or favoring by the United States Government, any agency thereof, or any of their contractors or subcontractors. The views and opinions expressed herein do not necessarily state or reflect those of the United States Government, any agency thereof, or any of their contractors.

SAND2009-0536
Unlimited Release
Printed January 2009

Novel Ultrafine Grain Size Processing of Soft Magnetic Materials

C. V. Robino, Multiscale Metallurgical Science and Technology Department
J. R. Michael, Materials Characterization Department

Sandia National Laboratories
P.O. Box 5800
Albuquerque, New Mexico 87185

Abstract

High performance soft magnetic alloys are used in solenoids in a wide variety of applications. These designs are currently being driven to provide more margin, reliability, and functionality through component size reductions; thereby providing greater power to drive ratio margins as well as decreases in volume and power requirements. In an effort to produce soft magnetic materials with improved properties, we have conducted an initial examination of one potential route for producing ultrafine grain sizes in the 49Fe-49Co-2V alloy. The approach was based on a known method for the production of very fine grain sizes in steels, and consisted of repeated, rapid phase transformation cycling through the ferrite to austenite transformation temperature range.

The results of this initial attempt to produce highly refined grain sizes in 49Fe-49Co-2V were successful in that appreciable reductions in grain size were realized. The as-received grain size was 15 μm with a standard deviation of 9.5 μm. For the temperature cycling conditions examined, grain refinement appears to saturate after approximately ten cycles at a grain size of 6 μm with standard deviation of 4 μm. The process also reduces the range of grain sizes present in these samples as the largest grain noted in the as received and treated conditions were 64 and 26 μm, respectively. The results were, however, complicated by the formation of an unexpected secondary ferritic constituent and considerable effort was directed at characterizing this phase. The analysis indicates that the phase is a V-rich ferrite, known as α_2, that forms due to an imbalance in the partitioning of vanadium during the heating and cooling portions of the thermal cycle. Considerable but unsuccessful effort was also directed at understanding the conditions under which this phase forms, since it is conceivable that this phase restricts the degree to which the grains can be refined. Due to this difficulty and the relatively short timeframe available in the study, magnetic and mechanical properties of the refined material could not be evaluated. An assessment of the potential for properties improvement through the transformation cycling approach, as well as recommendations for potential future work, are included in this report.

ACKNOWLEDGMENTS

The authors wish to thank Don Susan for his careful review of the manuscript, Paul Kotula for assistance in analytical electron microscopy, Alice Kilgo for expert metallographic sample preparation, and Bonnie McKenzie for scanning electron microscope support. The support of Dick Salzbrenner, the Laboratory Directed Research and Development program and its management, are also gratefully acknowledged.

CONTENTS

FIGURES

TABLES

ACRONYMS

AEM	analytical electron microscopy
BCC	body centered cubic
EBSD	electron backscatter diffraction
ECAP	equal channel angular pressing
EDS	energy dispersive spectroscopy
FCC	face centered cubic
FIB	focused ion beam
K-S	Kurjumov-Sachs orientation relationship
QIA	quantitative image analysis
SEM	scanning electron microscopy
TEM	transmission electron microscopy
WDS	wavelength dispersive spectroscopy

This page intentionally left blank.

1. INTRODUCTION

High performance soft magnetic alloys are used in solenoids in a wide variety of applications. Currently, these designs are being driven to provide more margin, reliability, and functionality through component size reductions; thereby providing greater power to drive ratio margins, as well as decreases in volume and power requirements. The primary material used for soft magnetic applications is the 49Fe-49Co-2V alloy Hiperco 50A (Hiperco is a registered trademark of Carpenter Technology Corporation, Reading PA). This alloy has historically demonstrated difficult machining and very low ductility when heat treated to maximize magnetic properties. The combination of difficult fabrication and poor mechanical properties makes the trend toward smaller electromechanical components problematic because brittle behavior affects fabrication, handling, and shock performance. More importantly, recent prototypic advanced development small stronglinks have displayed poorly performing solenoids, and design analysis indicated that substandard magnetic properties were likely the cause. Metallurgical analysis, using comparisons with larger solenoids that performed as expected, showed only a difference in grain size, but these could not be directly correlated with the reduced magnetic performance. Literature evaluations revealed critical gaps in knowledge concerning the relationships between microstructure and magnetic properties, so the current focus on decreasing component size is even more tenuous. In spite of their apparent chemical simplicity, heat treatment of these alloys is extremely complex and affects grain size, solid state phase transformations, ordering reactions, precipitation reactions, magnetic domain size, residual stress, impurity content, and crystallographic texturing. All these microstructural features interact in a non-linear, poorly understood, and often contradictory manner to control the magnetic and mechanical properties.

In a separate project, we are also exploring conventional heat treating approaches to improving properties and minimizing variability and uncertainty in 49Fe-49Co-2V. In the work reported here, we have attempted to produce and evaluate novel microstructures that can conceivably provide dramatic and quantum improvements in key properties. In particular, an attempt has been made to develop highly refined grain sizes . The basis for these enhancements is that ultrafine grain size materials have been shown to demonstrate interesting magnetic and mechanical behavior. For grain sizes smaller than the minimum domain size, the field required to reach magnetic saturation is significantly reduced. For example, it has been shown that Ni particles smaller than the minimum domain size reach saturation at fields that are about 25% of those required for larger grain sizes [Ref. 1]. This, of course, provides an immediate application advantage in that smaller windings or lower power will be required, or alternatively, greater drive torque margin can be derived at similar power. In turn, these provide greater system margin and decreased uncertainty. Further, when some metals are plastically deformed a subgrain structure and residual stress are developed [Ref. 2]. This stress causes a uniaxial magnetic anisotropy with the easy axis of magnetization parallel to the deformation axis. The aligning of the easy magnetization directions has been shown to increase the torque when strained materials are tested in a magnetometer. We have thus initiated an exploration into how these phenomena may be exploited in 49Fe-49Co-2V, and the key feature of the approach is to attempt to identify a basis for microstructural design (grain size) that is far removed from that used in conventional soft magnetic materials. Similarly, since mechanical failure in these alloys is typically by grain boundary failure, significant improvements in ductility are expected to be realized through grain size refinement and nano processing. The goal was to assess methods to

produce material in previously unexplored regions of microstructural "space" where dramatic improvements in properties are likely. Moreover, ultra-fine microstructural features are expected to be relatively insensitive to part size over a wide range of part sizes. The major risk in this concept is determination of the most suitable and feasible means for production of bulk ultrafine grained material. Possible routes to bulk ultrafine or nano-crystalline grain size include Equal Channel Angular Pressing (ECAP), friction stir processing, and solid state phase transformation cycling. Because ECAP and friction stir processing would all require substantial investments in time and resources, solid state phase transformation cycling was the focus of the current five month duration feasibility study.

Phase transformation cycling is a well known method for refining the grain size of iron based alloys [Ref. 3]. As shown in Figure 1, rapid cycling of steels between the high temperature face centered cubic austenite phase and the body centered cubic ferrite low temperature phase results in decreasing grain size as a function of the number of cycles. For the example shown, from a starting grain size of ASTM 6 (on the order of 40 μm), a very fine grain size of ASTM No. 12 (roughly 5 μm) was achieved within four transformation cycles.

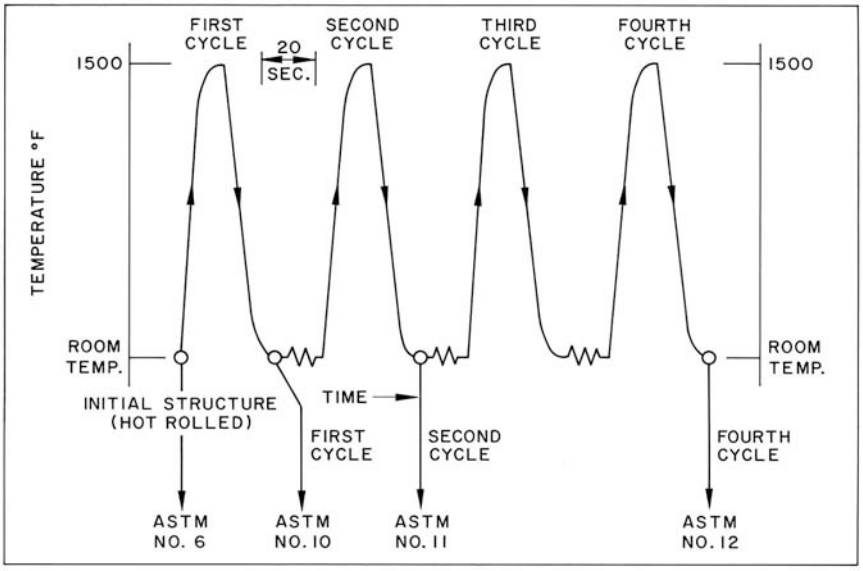

Figure 1. Schematic of grain size refinement method for steels [Ref. 3].

Although not steels *per se*, 49Fe-49Co-2V alloys are similar in that they transform to austenite at high temperature while ferrite is the stable phase at low temperatures. As a result, it was expected that phase transformation cycling would be an effective means to refine the grain size of 49Fe-49Co-2V alloys. No references regarding transformation cycling of 49Fe-49Co-2V or similar alloys were found.

If the approach is feasible and effective, it is certainly conceivable that the results of this work could be implemented in a relatively short timeframe. For example, many typical components are small, and thus production size quantities could conceivably be thermal cycled by using available induction heating methods, and this would not require a large infrastructure development program. Given the size of typical magnetic components, it is expected that if

effective, transformation cycling could be used to produce raw materials for real parts and applications.

Extensive microstructural characterization, including optical and scanning electron microscopy (SEM) coupled with electron diffraction to determine grain size, crystal structure, and crystallographic texture was used to guide the refinement experiments. Ultimately, once material with a suitable ultrafine grain structure has been produced and characterized microstructurally, this work will form the basis for more intensive follow-on development. This development would include magnetic and mechanical properties measurements to assess the efficacy of the grain refinement toward achieving new and expanded uses for the 49Fe-49Co-2V alloy.

2. EXPERIMENTAL PROCEDURES

2.1 Materials

The materials used in this investigation were two heats of 49Fe-49Co-2V (Hiperco 50A). The materials were obtained from war reserve (WR) stores at the Honeywell Federal Manufacturing Technologies – Kansas City Plant (FM&T-KCP) and are therefore representative of typical materials used for WR components and production. Material was in the form of 2.54 cm round bar in the mill processed (hot rolled and ground) condition. The compositions of the two heats are shown in Table 1.

Table 1. Composition of 49Fe-49Co-2V Heats

Element	Composition (wt%)	
	Heat 87456	Heat 98984
Co	48.80	48.82
V	2.03	1.99
C	0.004	0.002
Mn	0.03	0.08
Si	0.02	0.06
Cr	0.02	0.08
Ni	0.08	0.15
P	0.004	0.006
S	0.002	0.004
O	Not Reported	0.0030
N	Not Reported	0.0020
Fe	Balance	Balance

2.2 Grain Size Refinement Procedures

2.2.1 Transformation Temperatures

All thermal cycling experiments were conducted by using a Gleeble 3500 thermal-mechanical simulator. In this apparatus, 6.35 mm diameter rod samples were resistively heated under computer control while the sample diameter is continuously monitored by means of a laser extensometer. The freespan (length between water cooled copper jaws holding the test sample) was 19 mm. In order to determine the on-heating and on-cooling transformation temperatures initial experiments were conducted at a variety of heating and cooling rates from 2 to 50 °C/sec. The range of experimental conditions for the transformation temperatures are shown in Figure 2. Balanced heating and cooling rates, along with a 60 sec hold at the peak temperature of 1050°C were used. As shown in Figure 3, on-heating critical temperatures (start and finish of ferrite to austenite transformation, A_{c1} and A_{c3}), and on-cooling critical temperatures (start and finish of austenite to ferrite transformation, A_{r3} and A_{r1}) were determined graphically as the initial

deviations from, or the approach to, local linear expansion or contraction on the strain versus temperature records.

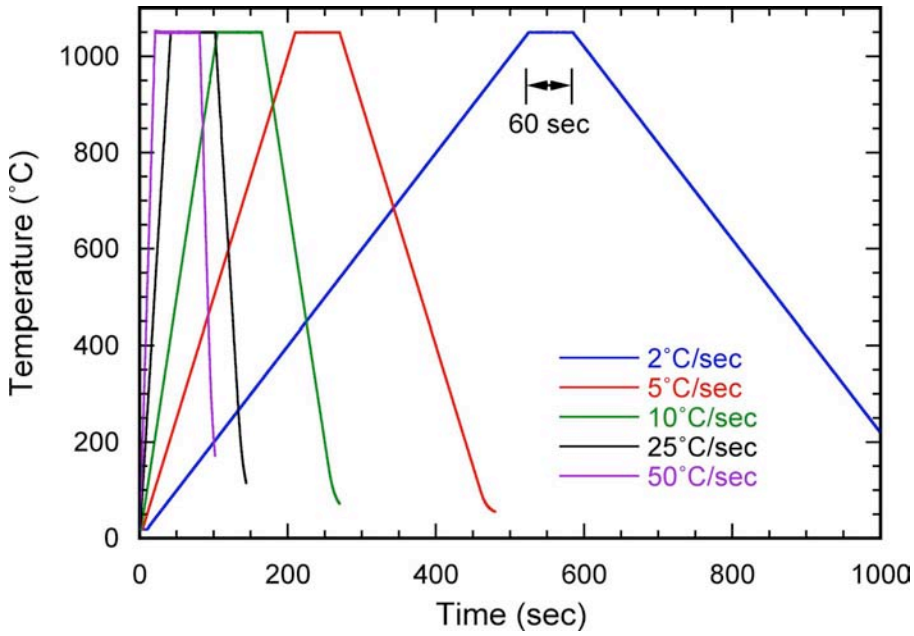

Figure 2. Temperature cycles used for the transformation temperature determinations.

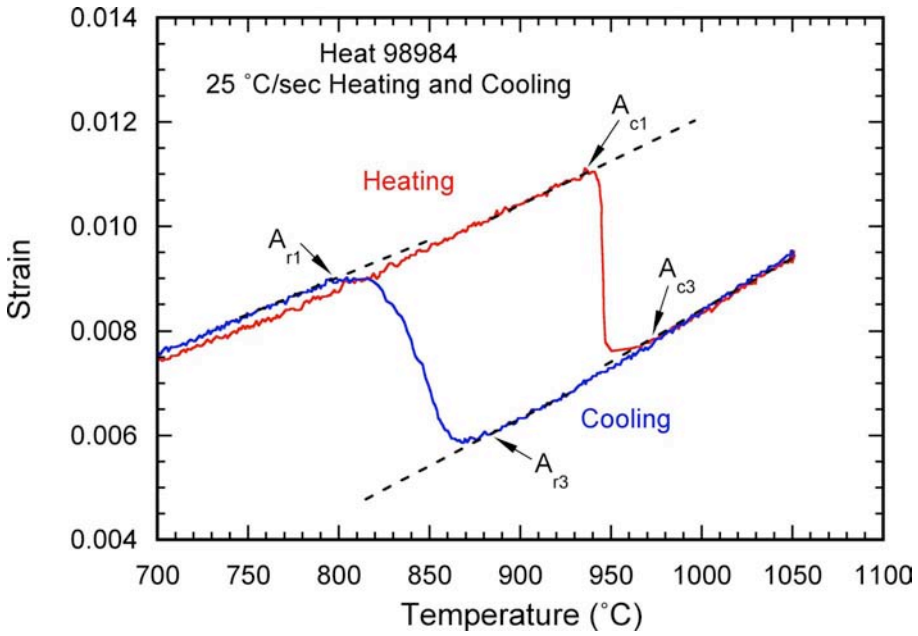

Figure 3. Determination of transformation start and finish temperatures.

2.2.2 Grain Refinement Temperature Cycling

The temperature limits used in the grain refinement temperature cycling experiments were selected based on the results of the critical temperature measurements and are shown in Table 2. Also shown are the heating and cooling rates used in the cycling. Balanced heating and cooling rates were generally used. Heat 87456 was used for the cycling experiments.

Table 2. Transformation Cycling Experiments

Heating Rate (C/sec)	Cooling Rate (C/sec)	Last Cycle Cooling Rate (C/sec)	High Cycle Temperature (C)	Low Cycle Temperature (C)	Number of Cycles
5	5	5	970	825	5
10	10	10	970		1
10	10	10	970	825	5
10	10	1 from 825	970	825	5
10	10	55 ave from 970-400	970	825	5
10	10	10	985	825	5
10	10	10	1000	825	5
10	10	10	970	825	10
10	10	10	970	825	20
10	10	10	1000	825	20
10	10	10	1000	600	20
10	10	10	970	600	20
10	10	10	950	600	20
10	10	10	945	600	20
10	10	10	948	600	20
10	10	10	925	825	20
40	40	40	970	825	10

In addition to the 6.35 mm diameter rod samples, limited initial thermal cycling experiments were conducted on large diameter hollow cylinders. These experiments were conducted in anticipation of the eventual need (assuming successful grain refinement) for magnetic properties determinations, and were therefore designed for provide a means for removal of magnetic core test samples as well as subscale mechanical test samples. A number of sample configurations were evaluated, with the most successful shown in Figure 4. Various compression loads were used, with 1000 lb showing the most repeatable and uniform circumferential heating.

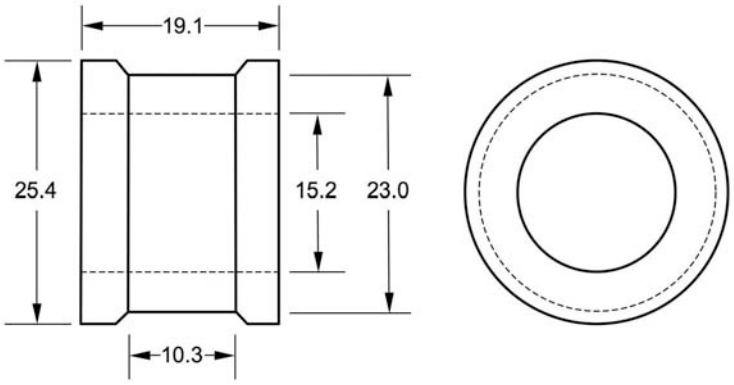

Figure 4. Large Gleeble test sample. Dimensions in mm.

2.3 Metallographic Analysis Procedures

The primary methods used for analysis of the refinement experiments were optical and electron microscopy. Light optical metallography was conducted on polished samples by using standard metallographic procedures. Electron backscattered diffraction (EBSD) was used to determine grain size, crystallographic orientation and texturing, and for the identification of phases present. Samples in the as-polished condition were examined in a Supra 55VP SEM with an HKL Technology Channel 5 EBSD system. Imaging was accomplished using a KE Development forward scatter detector positioned low on the EBSD phosphor screen [Ref. 4]. Microstructural imaging was also accomplished using band contrast, which is a measure of the relative contrast of the diffraction bands in a single EBSD pattern and can allow clearer delineation between grains within a phase than standard secondary or backscattered electron signals. The sample surface was tilted to 70° relative to the horizontal and analysis was completed at an accelerating voltage of 20 kV, a beam current of 2-3 nA, and a working distance of 13 mm. The acquired patterns were indexed against published crystallographic data [Ref. 5] to accurately distinguish between the face centered cubic (FCC) structure of austenite and the body centered cubic (BCC) of ferrite. Maps were created using a step size ranging from 0.05 μm- 0.2 μm depending on the minimum size of the features of interest in a given field of view. Mild levels of post processing were used to fill in unindexed pixels in the orientation maps shown here.

A limited transmission electron microscopy (TEM) study was also conducted on metallographic cross sections using the Focused Ion Beam (FIB) milling technique on an FEI DB235 system and thinned to electron transparency in situ. The samples were then removed and placed on a carbon film for insertion into an FEI Technai F30 equipped with an EDAX thin window spectrometer. Compositional mapping of Fe, Co, and V was accomplished using a 300kV accelerating potential.

3. RESULTS AND DISCUSSION

3.1 Grain Size Refinement

3.1.1 Transformation Temperatures

The results of the transformation temperature determinations for the two heats of 49Fe-49Co-2V alloy are shown in Figure 5, and the critical temperatures derived from these tests are summarized in Table 3. Over the range of rates examined, the transformation temperatures are not strong functions of heating or cooling rate. There are, however, appreciable differences between the two heats in terms of the finish temperature for the on-cooling transformation to ferrite, with Heat 98985 exhibiting significantly lower finish temperatures than Heat 87456. Given the close similarity between the compositions, Table 1, and starting grain sizes of the two heats, the reasons for this difference are not readily apparent.

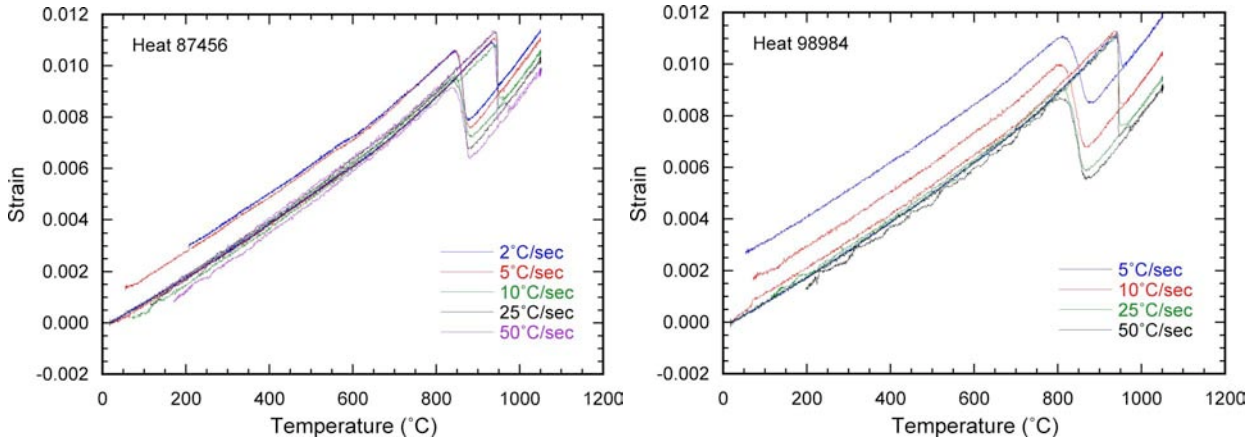

Figure 5. Dilatometry results for 49Fe-49Co-2V alloys. (a) Heat 87456. (b) Heat 98984.

Table 3. Transformation Temperatures for Heats 87456 and 98984

Heat Number	Heating Rate (°C/sec)	A_{c1} (°C)	A_{c3} (°C)	Cooling Rate (C/sec)	A_{r3} (°C)	A_{r1} (°C)
87456	2	930	957	2	891	841
	5	935	959	5	894	841
	10	939	965	10	891	843
	25	941	970	25	889	832
	50	938	976	50	892	833
98984	5	942	965	5	890	802
	10	936	966	10	884	797
	25	937	972	25	885	796
	50	937	977	50	885	788

As noted above, the transformation temperatures shown in Table 3 provided the initial basis for the temperature limits applied in the grain refinement experiments. Initial temperature limits were 825 and 970°C, but as testing progressed these limits were further adjusted and refined.

3.1.2 Grain Refinement Temperature Cycling

A typical dilatation (strain) versus temperature profile for a cyclic experiment is shown in Figure 6. The example shown is for 20 cycles between 600 and 1000°C at heating and cooling rates of 10 °C/sec. For this experiment, as well as the others listed in Table 2, there is little or no change in either the on-heating or on-cooling transformation temperatures as a function of the number of cycles. However, it is apparent that there is an overall increase and then decrease in the sample diameter (with the sample being slightly larger in diameter after the final cycle than initially). This change is also evident in Figure 7, which shows data from the same test plotted as strain and temperature as a function of time. This overall growth and contraction was highly variable depending on the details of the cycling, with some tests showing continuous growth as a function of the number of cycles. The data of Figure 7 can be interpreted as shown in Figure 8, which shows in greater detail the strains associated with the various ferrite (α) and austenite (γ) thermal expansion (or contraction) as well as the strains associated with transformations between the two phases.

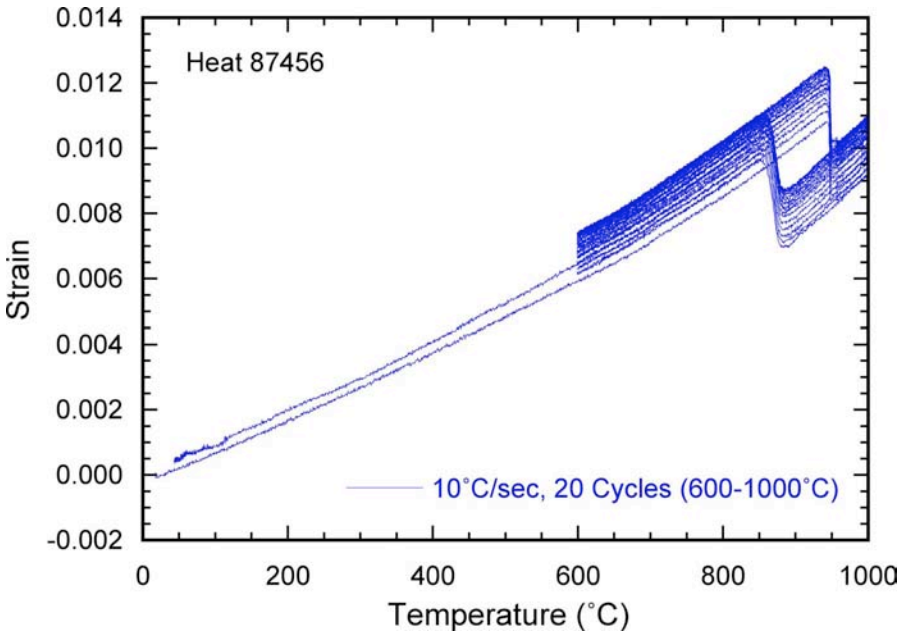

Figure 6. Typical strain versus temperature response for a cyclic grain refinement experiment.

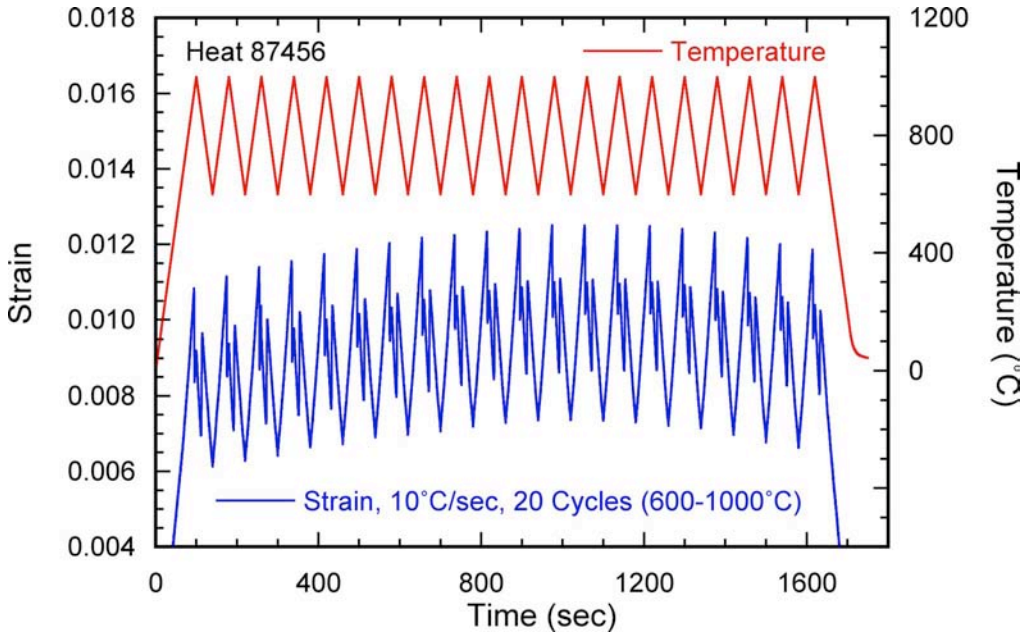

Figure 7. Typical strain and temperature versus time response for a cyclic grain refinement experiment.

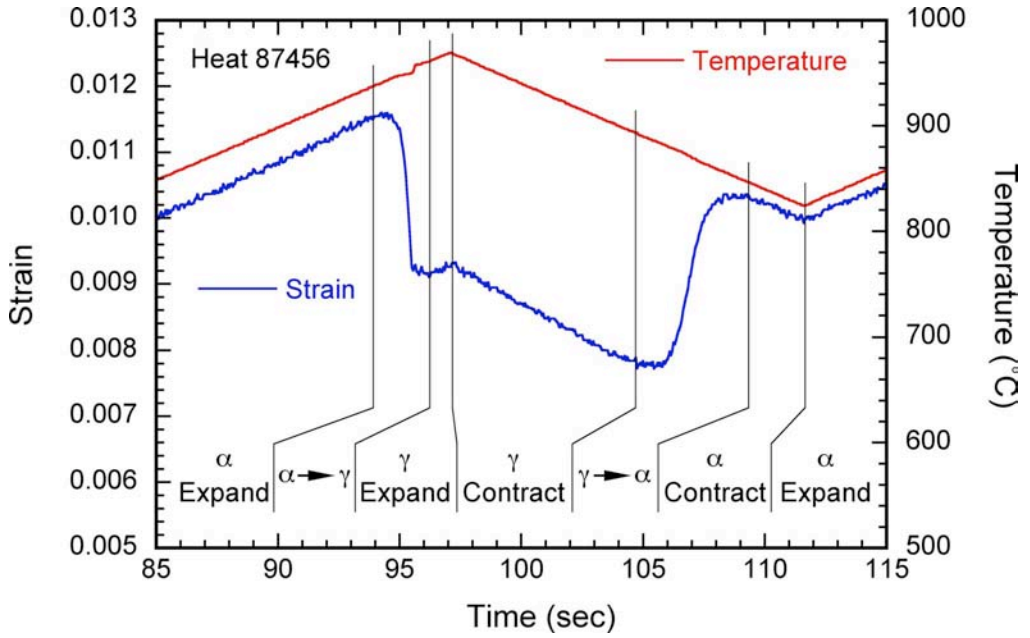

Figure 8. Basic interpretation of dilatation strain data (sample cycled between 825 and 970°C).

Figure 9 shows EBSD band contrast images of samples cycled at 10 °C/sec between 825 and 970°C. It is apparent that significant grain refinement is realized with a single transformation cycle at this rate. Further refinement occurs during subsequent cycling, although the refining effect appears to saturate after 10 cycles. Also apparent, however, is the formation of a

secondary phase (dark isolated regions) which is most prevalent in the sample cycled 20 times. For clarity, Figures 9(d) and 9(e) are reproduced on an enlarged scale in Figure 10.

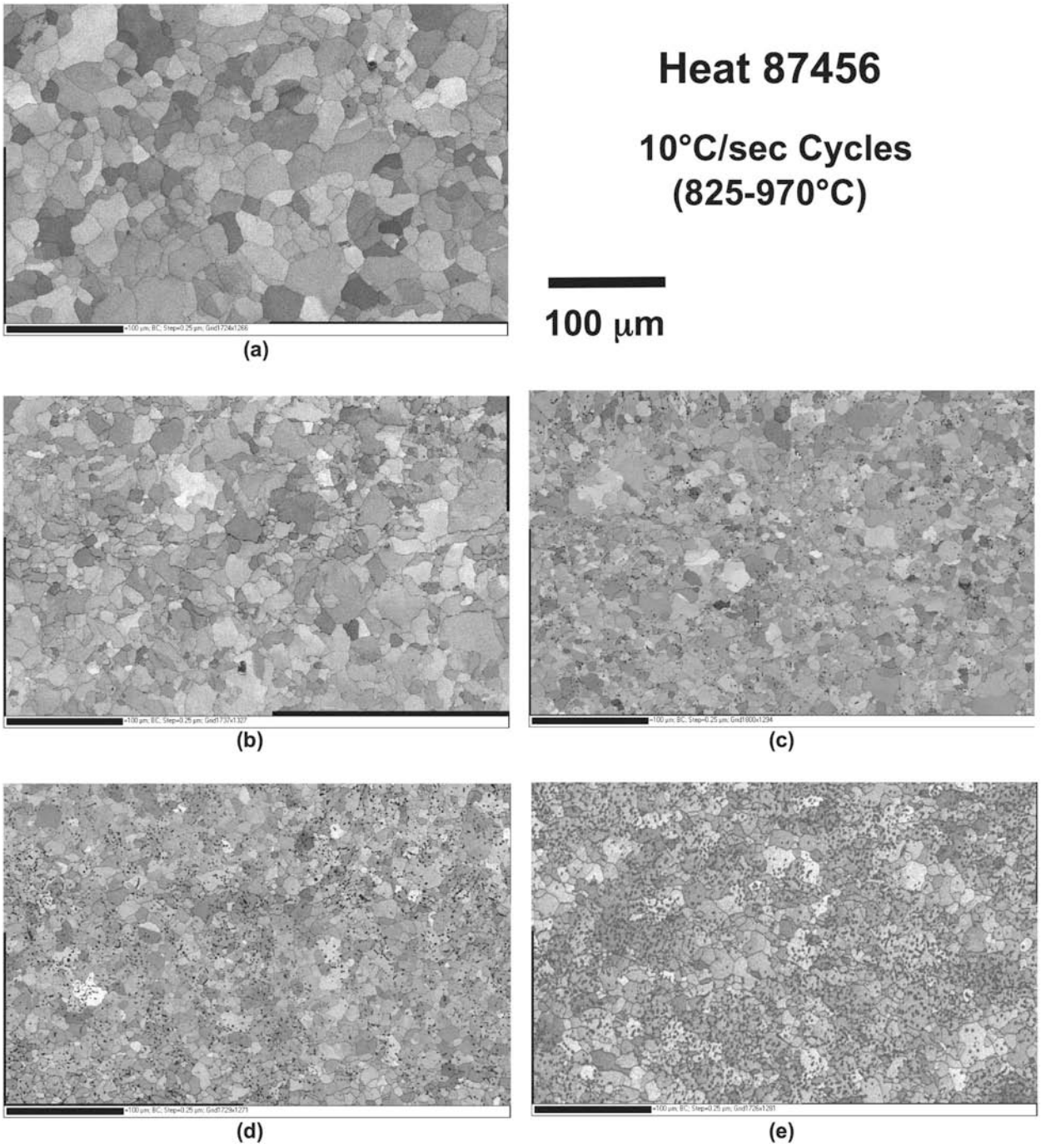

Figure 9. EBSD band contrast images for samples cycled between 825 and 970°C at 10°C/sec. (a) As-received, (b) 1 cycle, (c) 5 cycles, (d) 10 cycles, and (e) 20 cycles.

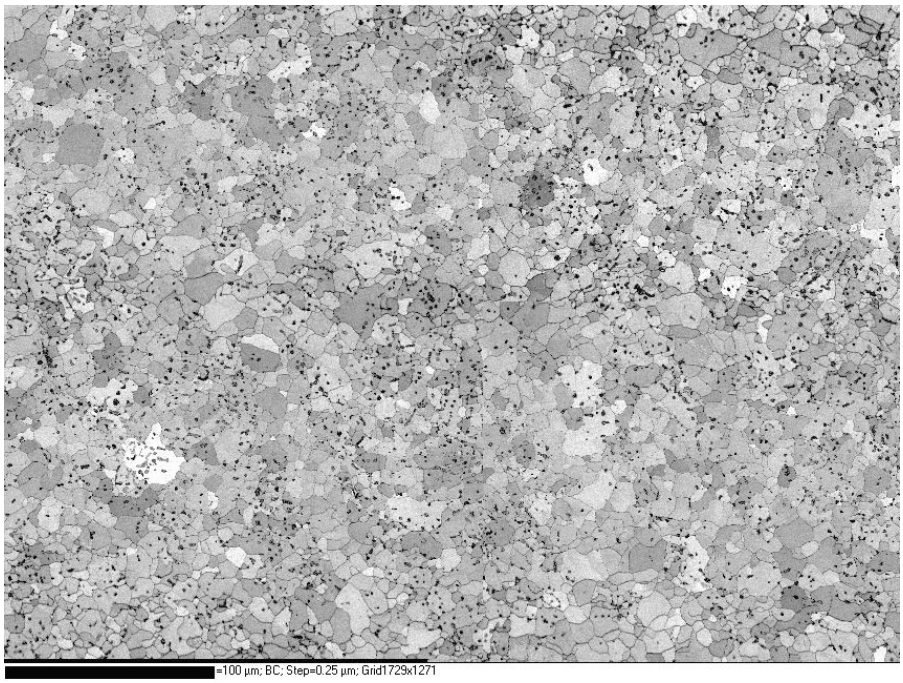

(a)

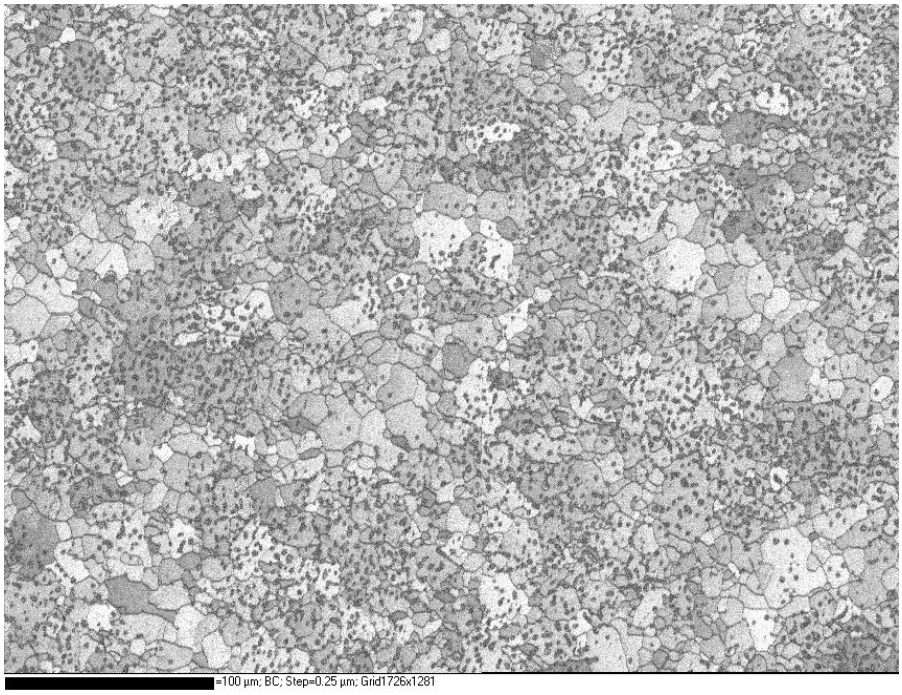

(b)

Figure 10. Enlargements of Figures 9(d) and 9(e) showing the saturation of grain refinement after 10 cycles and the development of a secondary constituent. Scale bars are 100 µm.

It is interesting to note that, as shown in Figure 9, the secondary constituent is not homogeneously distributed within the microstructure. In particular, Figure 9(a) shows that the features initially occur in banded groups (moving generally from the upper left to the lower right of the figure). The spacing between the bands is on the order of that expected for macrosegregation during ingot solidification, and it is therefore likely that the banding is associated with the segregation of V during original ingot casting at the producer. This characteristic of the secondary constituent, however, was not investigated further.

For a given cycling temperature range and cycling rate, the amount of second phase increases monotonically with the number of cycles as shown in Figure 11.

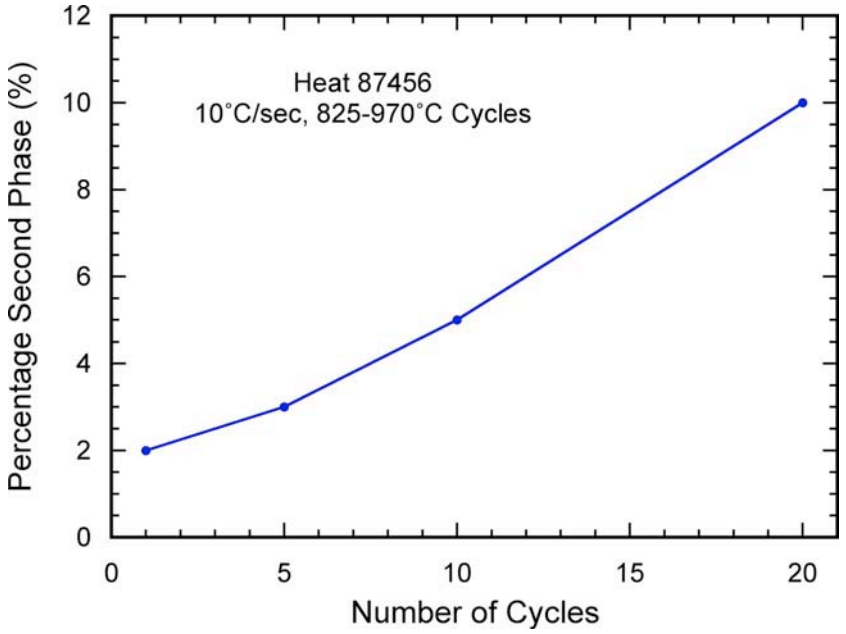

Figure 11. Percentage of secondary constituent as a function of the number of cycles for 10 °C/sec cycling between 825 and 970°C.

Higher resolution SEM images of the secondary constituent are shown in Figure 12. Although the phase is small, electron diffraction analyses indicted that the secondary constituent is body-centered cubic (ferrite or martensite). The constituent is distributed both within the ferrite matrix and occasionally along grain boundaries as shown by the arrows in the figure. In addition, there is substantial substructure visible within the constituent. The substructure implies the possibility that the constituent is martensitic in character. However, given the similar crystallography and unit cell dimensions between ferrite and low carbon martensite in Fe-Co-V alloys, the transformation mechanism cannot determined by measurement of the unit cell dimensions or simple observations of substructure. The nature of the secondary constituent and the transformation mechanisms by which it forms are discussed in more detail below.

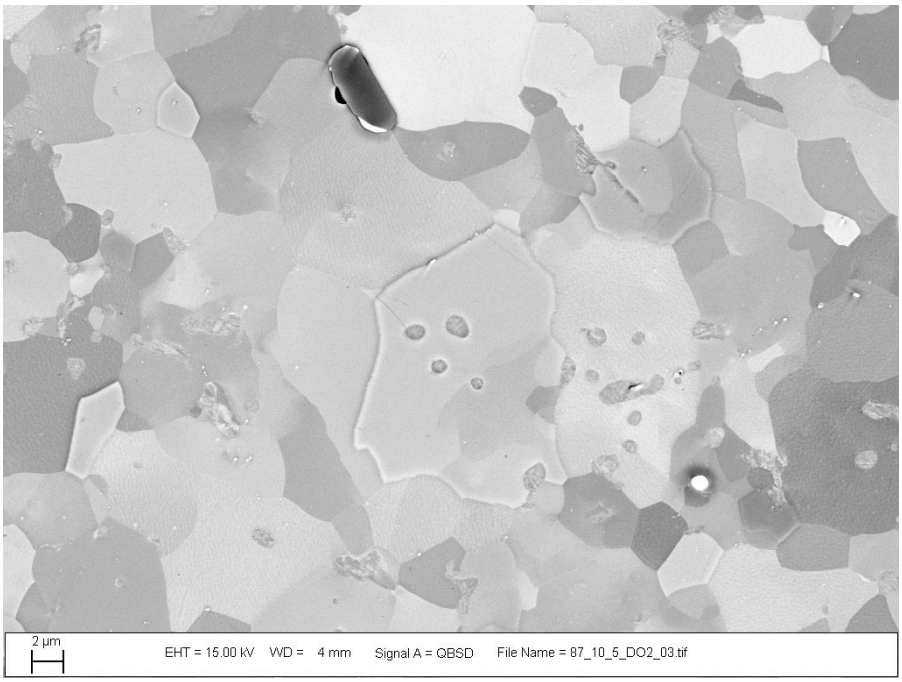

(a)

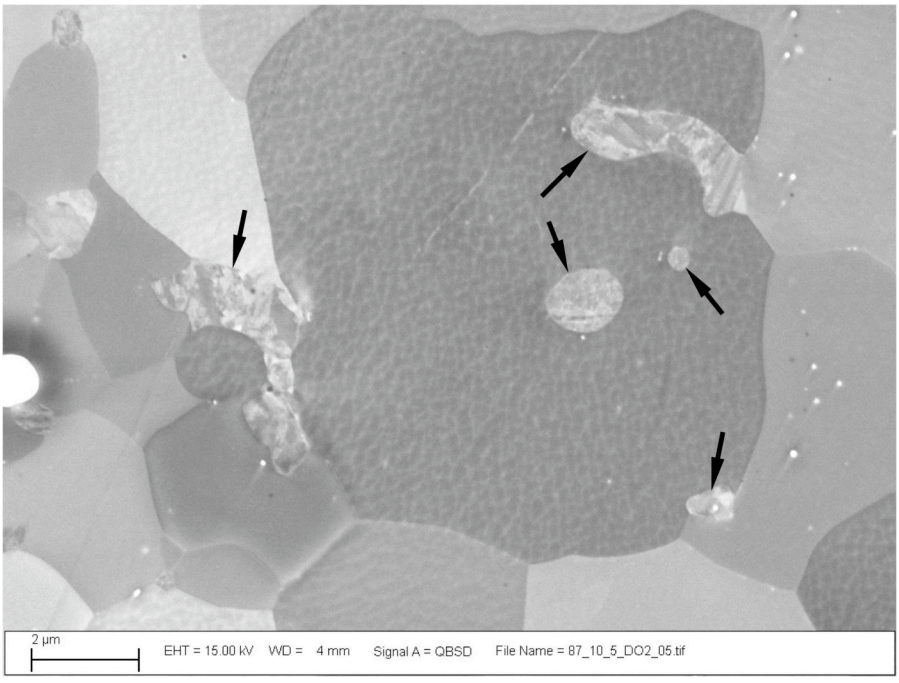

(b)

Figure 12. SEM backscattered images showing distribution, morphology, and substructure of the secondary constituent (arrows).

Further characterization of the secondary constituent was conducted by using TEM analysis. In this case, electron transparent TEM samples containing regions of the secondary constituent were extracted by using FIB techniques. The sample selected for this analysis had received 20

cycles between 825 and 1000°C at 10 °C/sec. The results of the compositional analysis are shown in Figure 13 and Table 4.

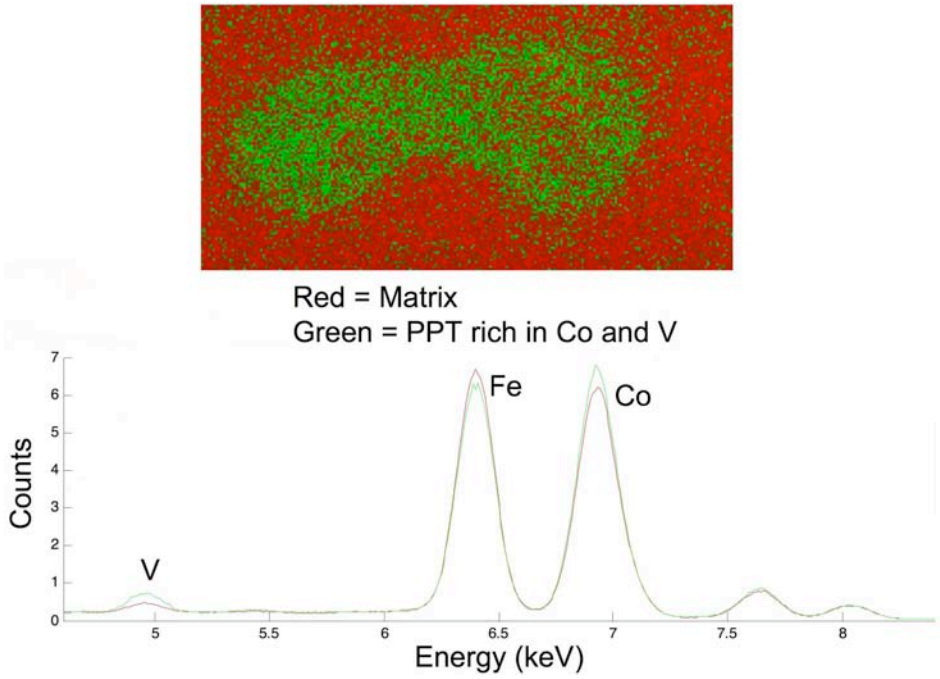

Figure 13. TEM spectral image and EDS spectra of secondary constituent.

Table 4. Compositions of matrix and secondary constituent in cycled 49Fe-49Co-2V alloy

Location	Fe (wt%)	Co (wt%)	V (wt%)
Matrix	51	48	1
Secondary Constituent	47	49	4

The compositional analyses indicate that, relative to the matrix, the secondary constituent is slightly enriched in Co and significantly enriched in V. Secondary constituents of this type have not been widely observed or reported in the literature. However, a similar phase has been observed and characterized by Bennett and Pinnel in a series of papers [Refs. 6-8]. In this case, the phase is a non-equilibrium BCC ferrite, denoted as α_2 by these investigators, and was formed during intercritical annealing in the two phase α_1 (disordered equilibrium ferrite) + γ (austenite) region of the phase diagram. The α_2 apparently forms from the γ (i.e. $\gamma \rightarrow \alpha_2$) during subsequent fast or intermediate rate cooling from the two-phase region, as was done in the current work. It is interesting to note that Pinnel and Bennett [Ref. 8] indicate good mechanical properties, and in particular ductility, for $\alpha_1 + \alpha_2$ microstructures. Based on microstructural evidence, Mahajan *et. al*. [Ref. 7] speculated that the $\gamma \rightarrow \alpha_2$ transformation proceeds by either a massive or martensitic mechanism, though they were not able to positively confirm either. Nevertheless, the

substructure within the α_2 regions in Figure 12 is consistent with their observations. The similarity in overall microstructure, composition, and substructure of the secondary constituent in the current work with those of the α_2 described by Bennett and Pinnel [Refs. 6-8] leads to the conclusion that the secondary constituent in the present study is α_2, a non-equilibrium BCC (ferrite) phase. This further implies that in the present cycling experiments partitioning of V occurs relatively rapidly to the remaining γ during cooling through the two phase region, thereby forming α_1 plus a V-rich γ (assuming that the microstructure is fully γ at the peak temperature). This latter assumption is supported by the observation that increasing the peak cycling temperature did not appear to significantly affect the formation of the secondary constituent.

Based on this assessment, the interpretation of the events during the cooling portion of the thermal cycling shown in Figure 8 can be modified slightly as shown in Figure 14. In this modification, it is postulated that during the cooling through the transformation temperature range in each cycle, as α_1 nucleates and grows, the remaining γ progressively increases in V content (denoted by γ_V). This enrichment process is consistent with the phase diagrams developed by Bennett and Pinnel [Refs. 6-8]. Stabilization (in a non-equilibrium sense) of the γ_V is presumed to occur because of the increasing stability of γ on cooling with increasing V content (i.e. the γ solvus temperature decreases with increasing V) and the decreasing mobility of V with decreasing temperature. Moreover, as the V content of the γ_V increases above 3 wt%, with subsequent cycles, γ is stabilized to low temperatures [Ref. 6]. Since the measured V content of the α_1 is near 4 wt% (Table 4) γ_V is thus stabilized to low temperature. The amount of γ_V is thought to increase during each cycle because of an imbalance in the manner in which V is redistributed during the transformation(s) on cooling and the transformation(s) and homogenization on heating.

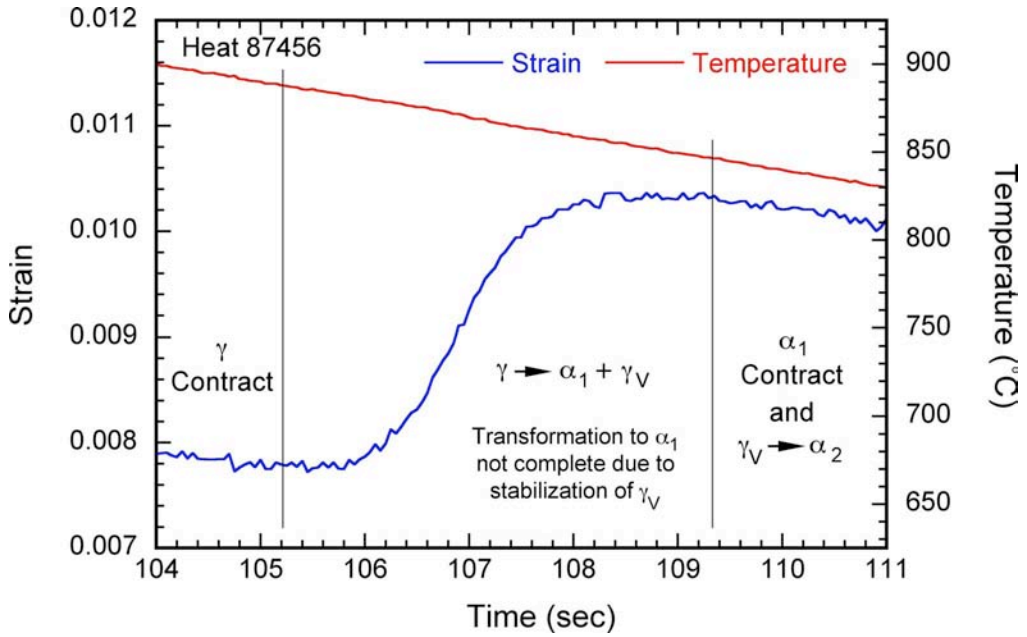

Figure 14. Modification of the interpretation of dilatation strain data during cooling portion of cycle (sample cycled between 825 and 970°C).

Further evidence for the increasing stabilization of the γ_V during cycling (and hence the increasing fraction of α_2 at room temperature with increasing number of cycles, Figure 11) can be seen in a series of tests conducted by using dynamic intercritical peak temperatures. In this case, the dynamic intercritical temperature range is considered to be the temperature range, at the heating rate of interest, over which the transformation to γ occurs. As shown in Figures 6 and 8, at 10 °C/sec the bulk of the transformation occurs rapidly over a very small temperature range (approximately 5°C) and as a result, such experiments are difficult to conduct. Nevertheless, comparison of the contraction during the $\alpha \rightarrow \gamma$ (or during later cycles the $\alpha_1 \rightarrow \gamma + \gamma_V$) as a function of the number of cycles is informative. Figure 15 shows the contraction associated with the on-heating transformations for several samples heated to different peak temperatures within the dynamic intercritical temperature range and for clarity only the first and final (20^{th}) cycles are shown. The selected peak temperatures vary only by 5°C , but they nevertheless capture a suitable range in terms of the amount of γ formed on the first cycle.

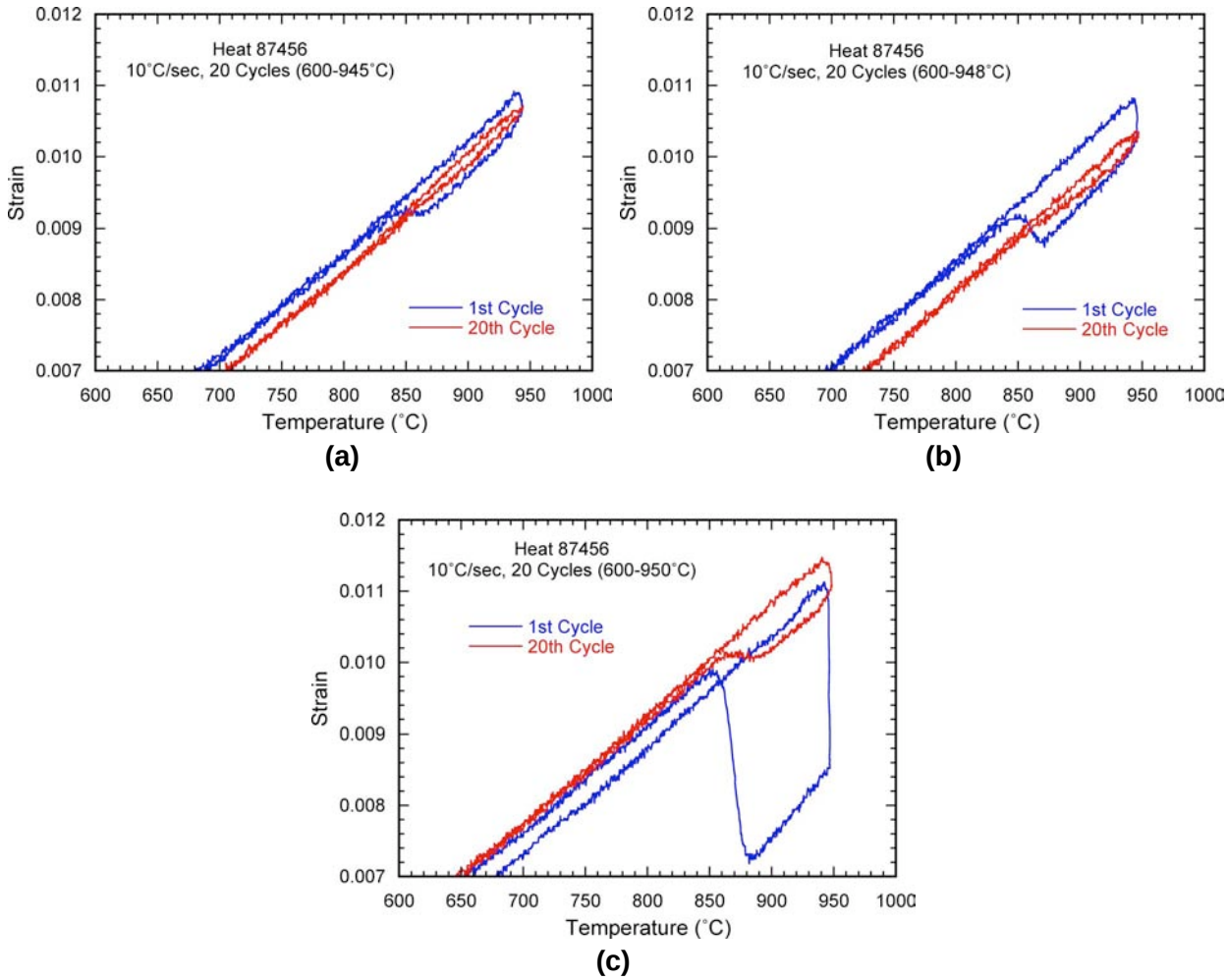

Figure 15. Strain versus temperature plots for samples heated and cycled at 10°C/sec between 600°C and peak temperatures in the intercritical temperature range. Peak temperatures are (a) 945°C, (b) 948°C, and (c) 950°C.

For each of the tests shown in Figure 15, the amount of austenite formed, as inferred from the magnitude of the contraction, on the first heating cycle is significantly greater than the amount formed on the final cycle. This observation implies that the bulk of the α (i.e. the α_1) is increasing in stability on heating. Since the γ solvus temperature increases with decreasing V concentration in 49Fe-49Co-2V alloys, this increasing stability of the α_1 is consistent with the progressive decreases in the V content of the α_1. This is essentially the compliment of the process described above for the increased stability of γ_V on cooling.

It is interesting to note that the $\gamma_V \rightarrow \alpha_2$ transformation, which must occur on cooling (at least during the final cooling cycle), is not readily evident in any of the dilatation records. As shown in Figure 10(b), the volume fraction of α_2 is substantial in many of the samples and thus it would normally be expected that the transformation would be visible as a discrete expansion or slope change in the strain versus temperature record. The initial heating and final cooling cycle for the sample of Figure 10(b) test is shown in Figure 16. Although there is some structure in the cooling curve at temperatures near 700°C, a similar slope change is also observed in the initial heating cycle. Since the order-disorder trans formation occurs near this temperature, it is likely that the slope change in both dilatation curves is the result of the order-disorder transformation and is not germane to the $\gamma_V \rightarrow \alpha_2$ transformation. Thus, the lack of other discrete changes in the dilatation curve would imply that the $\gamma_V \rightarrow \alpha_2$ transformation occurs gradually with cooling, rather than abruptly. In their microstructural study of the α_2 constituent, Mahajan *et. al.* [Ref. 7], was unable to determine if the transformation proceeded by either a martensitic or massive mechanism since the microstructure appeared to contain evidence of both mechanisms.

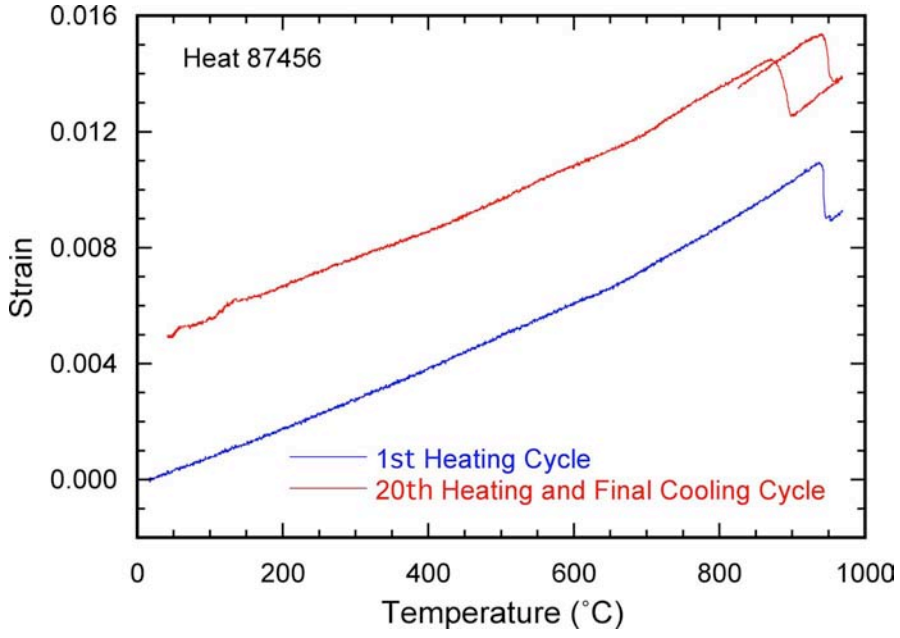

Figure 16. Initial heating and final heating and cooling cycle for sample cycled 20 times between 825 and 970°C.

As shown in Figure 17, the current work has employed EBSD analysis which allows the orientations of all the BCC variants within a single grain to be studied. In Figure 18, pole figures from the BCC α_2 constituent in Figure 17 are compared with pole figures calculated for the Kurjumov-Sachs (K-S) orientation relationships and it is apparent that the α_2 forms with all of the crystallographic variants associated with the K-S orientation relationships. This orientation relationship between austenite and ferrite is commonly associated with either martensite formation or a diffusive transformation [Ref. 9], while massive transformations do not have orientation relationships between the parent and the product phases. Thus, the current work clearly does not support the massive transformation mechanism for the $\gamma_V \rightarrow \alpha_2$ transformation. Final determination of whether the transformation occurs by a martensitic or diffusional decomposition mechanism, and over what cooling rate ranges either mechanism is operative, would require some additional study. For the cooling rate conditions evaluated here, however, the microstructural and crystallographic evidence strongly supports a martensitic transformation mechanism for the $\gamma_V \rightarrow \alpha_2$ transformation.

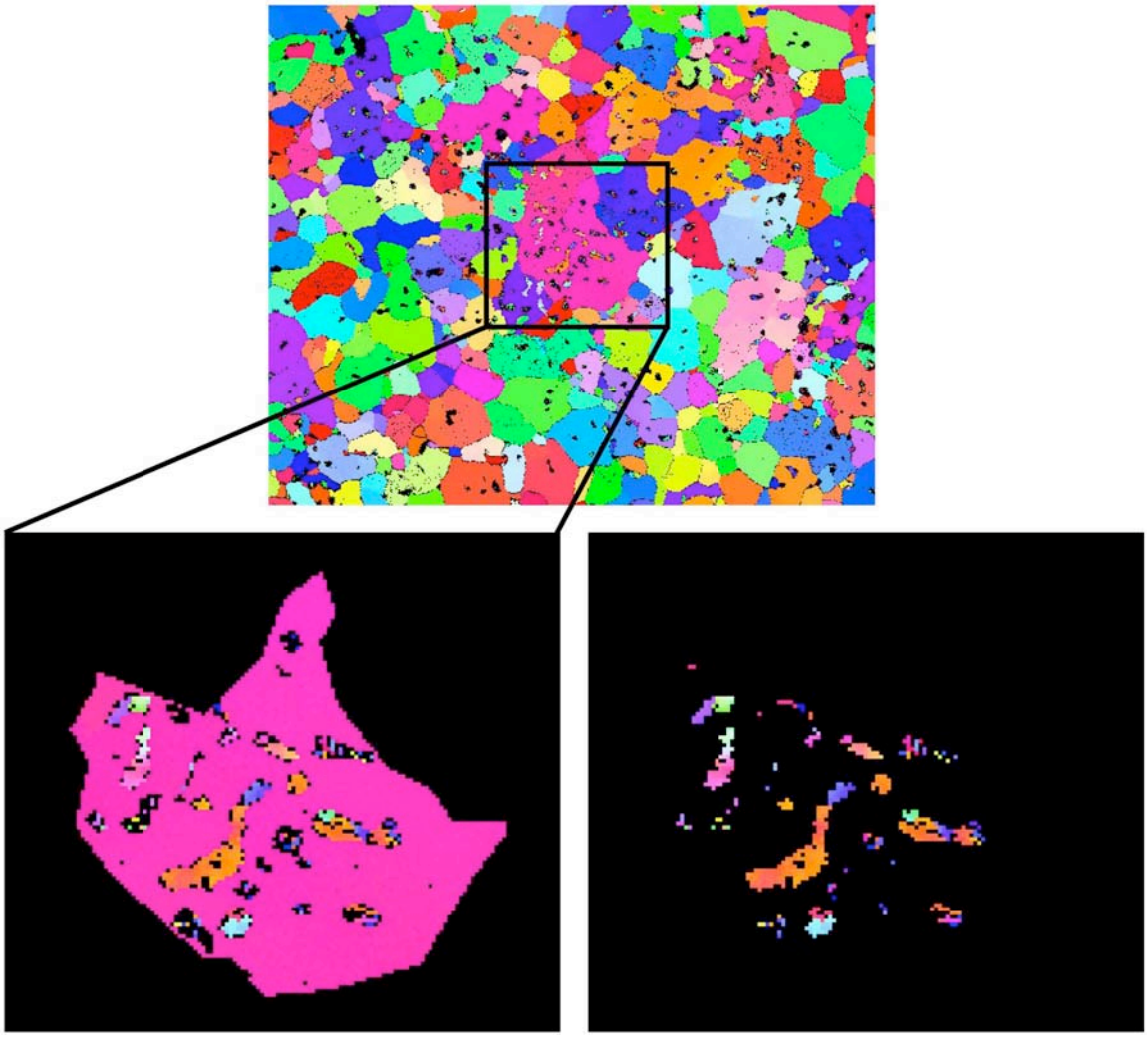

Figure 17. EBSD analysis on a single grain in sample cycled 10 times between 825 and 970°C. Lower right image shows EBSD pattern for α_2 constituent.

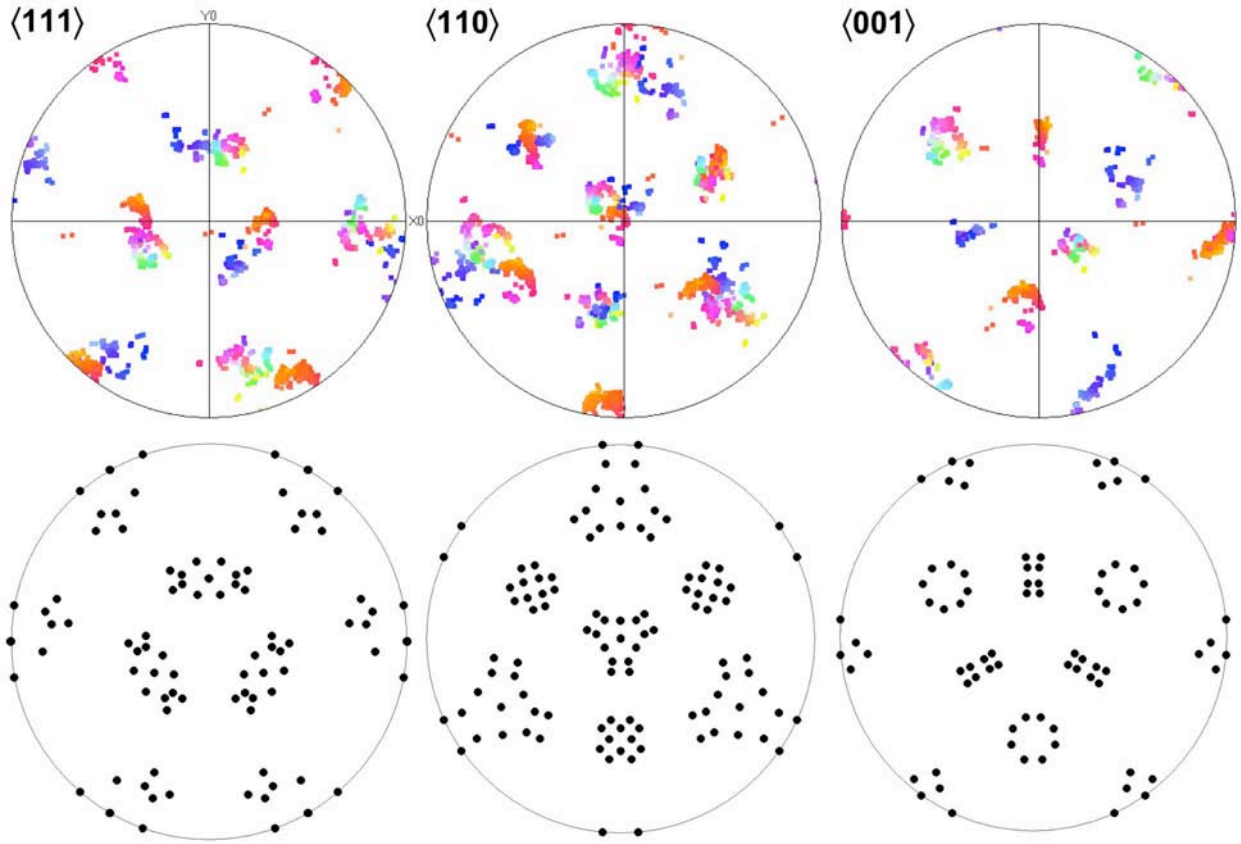

Figure 18. Pole figures in sample cycled 10 times between 825 and 970°C. The lower pole figures are calculated for the K-S orientation relationships.

3.2 Temperature Cycling of Large Samples

Unfortunately, within the time frame of this feasibility study, magnetic and mechanical properties measurements of cycled and grain refined material could not be conducted. In large part, this was due to the scoping nature of the experiments, which were primarily conducted on the small 6.35 mm diameter Gleeble samples that are not amenable to magnetic or mechanical properties measurement. Perhaps more importantly, however, the unexpected observation of the formation of the α_2 constituent and the large number of experiments that were initiated attempting to understand and control this constituent precluded the evaluation of properties. Initial evaluations of methods to transformation cycle samples that are suitable for magnetic and mechanical properties tests were, however conducted. These tests were largely successful, and should resources for future studies in this area become available, they are discussed here since they serve as the basis for the production of suitable test samples.

A variety of sample configurations and test conditions were evaluated in an attempt to maximize the sample volume while maintaining a suitable size and shape for the removal of magnetic test core laminations. The most successful of these was the hollow cylindrical sample configuration

shown in Figure 4. A series of still images extracted from a video record of a Gleeble test using this sample design is shown in Figure 19.

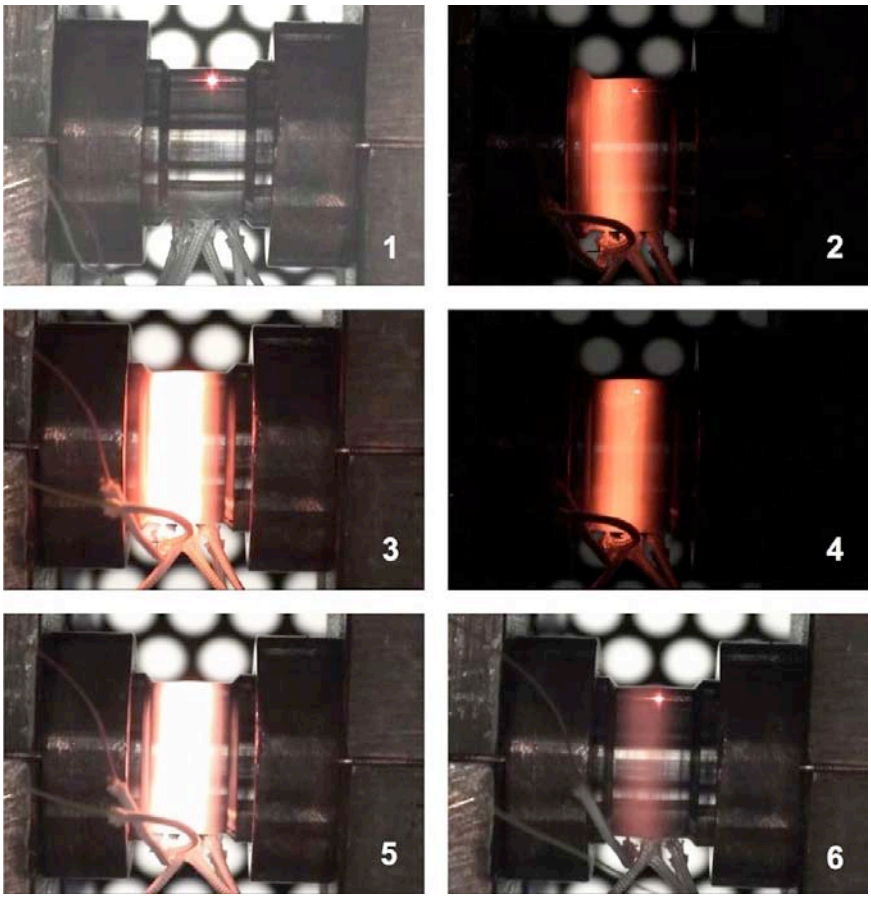

Figure 19. Still images at various times during test of hollow cylinder sample cycled 5 times between 825 and 970°C.

The sample was held by a compression load between water cooled Cu platens. A range of compressive loads was used, but it was observed that a minimum of 4450 N (1000 lb_f) was needed in order to ensure even heating around the circumference of the sample and to maximize the heating and cooling rate. The compressive load imparts a stress of about 6.9 MPa (6.3 ksi), but does not incur plastic deformation of the test sample at the peak temperatures evaluated. The configuration and test conditions were found to be capable of linear heating and cooling rates of at least 10°C/sec, which is comparable to the rate used for most of the testing on the smaller rod samples in this study.

The images of Figure 19 illustrate that there is a temperature gradient along the length of the test sample. This gradient is a characteristic of resistance heating and is common to all Gleeble thermal cycling. It should also be noted that the images indicate that the hot zone is shifted toward the left side of the reduced section. This shift is a consequence of the fact that in its current configuration, cooling water flows from the right hand platen to the left platen. Since the electrical current required to heat a sample of this size is relative high, the cooling water exiting

the right side platen is effectively preheated prior to entering the left platen. This imbalance can easily be rectified in future studies by flowing the cooling water in parallel, rather than series, through the jaws. In order to characterize the position, length, and uniformity of the hot zone, a number of tests using multiple thermocouples were conducted. These tests indicated that the length of the uniformly heated (± 10°C) zone provides sufficient material for the fabrication of magnetic test core samples.

4. SUMMARY AND IMPLICATIONS

In this study, we have conducted an initial examination of one potential route for producing ultrafine grain sizes in an important soft magnetic alloy. The approach was based on a known method for the production of very fine grain sizes in steels, and consisted of rapid and repeated thermal cycling through the ferrite to austenite phase transformation temperature range.

The results of this initial attempt to produce highly refined grain sizes in 49Fe-49Co-2V were successful in that appreciable reductions in grain size were observed. The grain refinement appears to saturate after approximately ten cycles at a grain size of 6 μm. The results were, however, complicated by the formation of an unexpected secondary ferritic constituent and considerable effort was directed at characterizing this phase. The analysis indicates that the phase is a V-rich ferrite, known as α_2, that forms due to partitioning of V to the remaining γ during the cooling phase of the cycle. Considerable effort was also directed at understanding the conditions under which this phase forms, since it is conceivable that this phase restricts the degree to which the grains can be refined. This effort included examination of numerous cyclic minimum and maximum temperatures, as well as a range of heating and cooling rates within the range where grain size refinement can be realized. The range of conditions was also constrained by the desire to insure that they be achievable in actual practice for real applications. In any case, the phase was observed to exist under all cycling conditions that were examined. Clearly, in the time frame associated with this feasibility study, an exhaustive search for possible conditions that preclude α_2 formation could not be accomplished. Nevertheless, on the basis of what is now known about this phase, it is important to consider what options might be available should additional work be undertaken in the future.

Since it is believed that the phase forms because of an imbalance in the manner in which V is redistributed during on-cooling and on-heating transformations, it seems likely that unbalanced heating and cooling rates during each cycle may provide one means for controlling its formation. In particular, because the V partitions to the remaining γ during cooling and this segregation is apparently not reversed during subsequent heating, it appears likely that higher rates during cooling coupled with lower rates during heating might offset this imbalance. To a first approximation, the relative rates of cooling and heating would be essentially a ratio of the rates of V diffusion in ferrite and austenite in the temperature of interest, i.e. rate of V diffusion in ferrite during the on cooling transformation versus the rate of V diffusion in austenite during the on heating transformation as well as any heating above this temperature. Roughly speaking, temperatures of interest for V diffusion in ferrite would appear from Table 1 to be 830-890°C, while the temperature for of interest for V diffusion in austenite would be near 970°C and above. Based on data for the diffusion of V in Fe [Ref. 10], it would appear that the cooling rates would

have to be on the order of 15-20 times faster than the heating rates in order to offset the imbalance in V diffusion. Clearly, this estimate is extremely approximate, but nevertheless provides at least a starting point to guide experimentation should continued evaluation be possible. Unfortunately, since it is the heating rate that must be slow relative to the cooling rate, the possibility of grain growth in both the ferrite and austenite during heating may negate any potential refining due to cycling. From Table 3 it is apparent that there are differences in the transformation temperatures between the two available heats, so that the effect of composition on refinement should also be evaluated. In addition, deformation during the cycling could also be used to affect the progress of the transformations and the level of grain refinement.

Another potential but related method that could be examined in future evaluations is the use of extremely high rates during the cooling portion of the cycle, so that the diffusional transformation of γ to $\alpha_1 + \gamma_V$ is superceded by a martensitic transformation. 49Fe-49Co-2V alloys with a uniform V concentration of 2 wt% throughout the γ require, however, rapid quenching (iced-brine even in moderate section sizes), so this approach may be difficult to accomplish in practical situations. In any case, it is clear that there are a number of potential areas that require investigation, but extensive experimentation is likely required to achieve dramatic grain refinement and sub-micron grain sizes.

Although it was not possible in the time frame of the study to measure either the magnetic or mechanical properties directly, the refinement in grain size is expected to have a positive effect on both strength and toughness. However, given the presence of the α_2 constituent, it is also important to consider what effect the α_2 might have on these properties. In their study of intercritically annealed 49Fe-49Co-2V alloys, Pinnel and Bennett [Ref. 8] observed ductile fracture with appreciable necking for all $\alpha_1 + \alpha_2$ two phase microstructures independent of phase fractions or vanadium content. From this observation, it is surmised that the microstructures developed in the current cycling study would also exhibit ductile behavior. Pinnel and Bennett [Ref. 8] also conducted tensile tests on material aged at 600°C, and while the strength increased, elongation to failure did not appear to be reduced. Necking was not observed in aged material, however, and the material failed by brittle cleavage after only uniform elongation. This was attributed to both crystallographic ordering and fine, stable γ precipitates formed by decomposition of the α_2. The magnetic property results of Pinnel and Bennett [Ref. 8], are difficult to interpret with respect to the current study, however. This difficulty is primarily a result of the fact that they were not attempting to optimize soft magnetic properties, but rather were attempting to produce hard magnetic materials. We thus, unfortunately, do not have any reasonable basis for estimating the effects of the temperature cycling, grain refinement, and α_2 formation on magnetic properties. At this stage in the development cycled and grain refined 49Fe-49Co-2V alloys, therefore, the magnetic characteristics of the microstructures developed in this study must be considered unknown.

5. REFERENCES

1. C. Kittel, J. K. Galt and W. E. Campbell, “Crucial Experiment Demonstrating Single Domain Property of Fine Ferromagnetic Powders”, *Physical. Review*, Vol. 77,(1950), p. 725.

2. R. H. Yu, S. Basu, y. Zhang, A. Parvisi-Majidi, and J. Q. Xiao, “Pinning Effect of Grain Boundaries on Magnetic Domain Wall in FeCo bases magnetic Alloys”, Journal of Applied Physics, Vol. 85, No. 9, (1999), p. 6655.

3. H. E. McGannon, *Making, Shaping, and Treating of Steel*, United States Steel Press, Pittsburgh, (1971), p. 1106.

4. D. J. Prior, et al., “Orientation Contrast Imaging of Microstructures in Rocks using Forescatter Detectors in the Scanning Electron Microscope”. Mineralogical Magazine, 1996. 60(403): p. 859- 869.

5. T. Hahn, *International Tables for Crystallography*. 1996.

6. J. E. Bennett and M. R. Pinnel, “Aspects of Phase Equilibria in Fe/Co/2.5 to 3.0% V Alloys”, *Journal of Materials Science*, Vol. 9, (1974), 1083-1090.

7. S. Mahajan, M. R. Pinnel, and J. E. Bennett, “Influence of Heat Treatment on Microstructures in and Fe-Co-V Alloy”, *Metallurgical Transactions*, Vol. 5, (1974), pp 1263-1272.

8. M. R. Pinnel and J. E. Bennett, “Correlation of Magnetic and Mechanical Properties with Microstructure in Fe/Co/2-3 pct V Alloys”, *Metallurgical Transactions*, Vol. 5, (1974), pp 1273-1783.

9. J .I. Goldstein and J. R. Michael, “The Formation of Plessite in Meteoritic Metal”, Meteoritics and Planetary Science, Vol. 41, No. 4, (2006), p. 553-570.

10. E. A. Brandes, *Smithells Metals Reference Book, Sixth Edition*, Butterworths, London, (1983), pp13-66 and 13-90.

DISTRIBUTION

1	MS 0110	C. J. Barbour	8340
1	MS 0123	D. L. Chavez, LDRD Office	1011
1	MS 0885	J. E. Johannes	1810
1	MS 0885	R. J. Salzbrenner	1820
1	MS 0889	F. M. Hosking	1813
1	MS 0889	D. F. Susan	1813
5	MS 0889	C. V. Robino	1813
5	MS 0886	J. R. Michael	1822
1	MS 0899	Technical Library	9536 (electronic)